Observed and Modeled Pathways of the Iceland Scotland Overflow Water in the eastern North Atlantic

Sijia Zou, Susan Lozier, Walter Zenk, Amy Bower, William Johns

Abstract

The spreading of Iceland Scotland Overflow Water (ISOW) in the eastern North Atlantic has largely been studied in an Eulerian frame using numerical models or with observations limited to a few locations. No study to date has provided a comprehensive description of the ISOW spreading pathways from both Eulerian and Lagrangian perspectives. In this paper, we use a combination of previously unreported current meter data, hydrographic data, RAFOS float data, and a high resolution (1/12°) numerical ocean model to study the spreading pathways of ISOW from both of these perspectives. We identify three ISOW transport cores in the central Iceland Basin (~59°N), with the major core along the eastern boundary of the Reykjanes Ridge (RR) and the other two in the basin interior. Based on trajectories of observed and/or numerical floats seeded along 59°N, we also describe the ISOW spreading pathways and quantify their relative importance. Within 10 years, 7-11% of ISOW from 59°N escapes into the Irminger Sea via gaps in the RR north of the Charlie Gibbs Fracture Zone (CGFZ); the water that moves through these gaps principally originates from the shallower ISOW layer along the RR eastern boundary. 10-13% travels further southward until the CGFZ, where it crosses westward into the western subpolar gyre. 18-21% of ISOW spreads southward along the eastern flank of the Mid-Atlantic Ridge into the Western European Basin (WEB). Most of the remaining water stays in the Iceland Basin over the 10-year period. A model-based investigation provides a first look at the temporal variability of these ISOW pathways. We find that the fraction of southward water exported into the WEB is anti-correlated with the export through the CGFZ, a result assumed to reflect these pathways' interactions with the North Atlantic Current in magnitude and/or position shift.

1. Introduction

Iceland Scotland Overflow Water (ISOW), one of the major components of the lower limb of the Atlantic Meridional Overturning Circulation (AMOC), is formed in the Nordic Seas from these identified sources: open-ocean convection in the Greenland Sea, dense water formation along the Arctic shelves and the transformation of Atlantic water (Rudels et al., 1999; Eldevik et al., 2009). After formation, ISOW flows to the eastern subpolar gyre mainly through the Faroe-Shetland Channel, with a small portion over the Iceland-Faroe Ridge. ISOW entrains the ambient water as it spreads southward primarily along the slope of the northwest Iceland Basin and then out into the eastern North Atlantic (Fleischmann et al., 2001; van Aken and de Boer, 1995).

An understanding of the distribution and variability of ISOW spreading pathways, together with the other two components of the lower limb of the AMOC, the Labrador Sea Water (LSW) and Denmark Strait Overflow Water (DSOW), is fundamental to our understanding of AMOC structure and variability.

Traditionally, the Deep Western Boundary Current (DWBC) was considered the major conduit from the subpolar to the subtropical gyre for these deep water masses. As a consequence of this assumption, DWBC transport variability was roughly equated to variability of the deep AMOC limb (Molinari et al., 1998; Curry et al., 1998; Schott et al., 2006). However, recent studies have demonstrated the importance of interior pathways in exporting LSW (Bower et al., 2009; Lavender et al., 2005; Gary et al., 2012) and the overflow waters (Xu et al., 2015; Lozier et al., 2013; Gary et al., 2011; Stramma et al., 2004) to the subtropical gyre in the western North Atlantic, thus calling into question the DWBC as the sole conduit of deep water masses in the North Atlantic. Besides an interior pathway for overflow waters in the western North Atlantic, studies based on models and Lagrangian floats have identified a southward interior pathway of ISOW along the eastern flank of the Mid-Atlantic Ridge (MAR) (Xu et al., 2010; Machín et al, 2006; Lankhorst and Zenk, 2006).

In addition to the southward branch along the eastern flank of the MAR, two other ISOW spreading pathways have also been identified in the eastern North Atlantic: one via gaps in the Reykjanes Ridge (RR) north of the Charlie Gibbs Fracture Zone (CGFZ), and the other via a westward crossing through the CGFZ. The former branch has been mostly studied with models (Xu et al., 2010; Chang et al., 2009), while the latter branch has been studied using both model output (Xu et al., 2010; Chang et al., 2009) and current meter measurements (Saunders, 1994; Bower and Furey, 2017). In both cases, the pathways are deduced from Eulerian data.

Though these prior Eulerian studies identified particular ISOW pathways, no study to date has validated these pathways from a Lagrangian perspective, primarily because Lagrangian data has been so limited. Additionally, no previous study has assessed the temporal interplay among the spreading branches. Thus, the goals of this paper are to: 1) provide a comprehensive description of the ISOW spreading pathways in a combined Eulerian and Lagrangian frame; 2) shed light on the interplay between spreading pathways on interannual time scales. Specifically, we use previously unreported current meter data from two different arrays, two sets of CTD stations, RAFOS float data and a high resolution model output to: 1) identify ISOW in the Iceland Basin; 2) trace different ISOW spreading pathways; 3) quantify the volume transport and measure the relative importance of different ISOW branches; and 4) assess the temporal variability of the spreading pathways.

The paper is organized as follows: We review ISOW pathways from previous studies in section 2 and summarize our data sources and methods in section 3. In section 4, we provide a comprehensive description of the major ISOW export pathways out of the Iceland Basin and in section 5, we quantify the different pathways from both Eulerian and Lagrangian perspectives. Conclusions follow in section 6.

2. Prior knowledge of the Iceland Scotland Overflow Water pathways and their transports

Iceland Scotland Overflow Water (ISOW) enters the eastern subpolar North Atlantic between Iceland and Scotland primarily through the Faroe-Shetland Channel (FSC) (Hansen and Østerhus, 2007) and a minor part over the Iceland-Faroe Ridge (Beaird et al., 2013) (**Figure 1**). After flowing through the FSC, one ISOW branch flows into the Iceland Basin through the Faroe Bank Channel,

filling the bottom layer (density ≥ 27.80 kg/m^3 with a depth range from 1300m to the bottom) on the Icelandic Slope (Saunders, 1996; Kanzow and Zenk, 2014; Xu et al., 2010). Another branch travels southward into the Rockall Trough across the Wyville-Thomson Ridge (WTR) (Chang et al., 2009; Ellett and Roberts, 1973; Sherwin and Turrell, 2005). A small branch flows southward west of the Maury Channel (Chang et al., 2009; Xu et al., 2010). As ISOW spreads southward and westward, it mixes with lighter subtropical waters carried by the North Atlantic Current (NAC), Labrador Sea Water (LSW) from the western subpolar gyre, and Lower Deep Water (LDW) from the south (van Aken 1995; McCartney, 1992).

Direct measurements of the transport in the ISOW layer are available at limited locations (labeled in magenta in **Figure 1**). The FBC overflow is measured to be 2.1-2.2 Sv (1 Sv = 10^6 m^3/s) (Hansen and Østerhus, 2007; Hansen et al., 2016) and the overflow over the IFR is estimated to be > 0.8 Sv (Beaird et al., 2013). A southward transport of 3.2-3.8 Sv is observed in the ISOW layer along the northwestern slope of the basin south of Iceland (Saunders, 1996; Kanzow and Zenk, 2014). A transport of 0.1-3.0 Sv with large uncertainties through the Rockall Trough is estimated by Dickson and Brown (1994), while a more recent study shows that the transport across the WTR is at the lower bound of the range (Sherwin et al., 2008). A westward transport of waters in the ISOW layer across the Charlie Gibbs Fracture Zone (CGFZ), measured with mooring arrays, is 1.7-2.4 Sv (Saunders, 1994; Bower and Furey, 2017). However, this branch is highly variable due to the frequent approach of the eastward-flowing NAC (Schott et al., 1999; Bower and Furey, 2017), whose deep flow field interacts with the westward transport of ISOW. The transport of waters denser than 27.80 kg/m^3 in the southward branch along the eastern MAR flank from the Iceland Basin to the West European Basin (WEB) has been estimated to be 2.4-3.5 Sv from tracer data (Fleischmann et al., 2001).

In addition to the Eulerian-based studies, past Lagrangian studies have also investigated the spreading of intermediate and deep waters in the Iceland Basin. With passive neutrally buoyant RAFOS floats (released between 1419 to 2866 dbar), Lankhorst and Zenk (2006) identify three major pathways of LSW in the Iceland Basin: westward escape into the Irminger Sea through the Bight Fracture Zone (BFZ) along the RR (see also Bower et al., 2002); eastward flow across the CGFZ, which is the major exchange gateway of LSW between the Irminger Sea and the Iceland Basin; and a southward spreading along the eastern flank of the MAR (see also Machín et al., 2006). Though these pathways are mostly identified in the LSW layer, which is shallower than the ISOW layer, the pathways across the RR gaps and along the eastern flank of the MAR are similar to those observed in the ISOW layer (as detailed below), indicating a barotropic structure for the spreading of intermediate and deep waters.

A number of modeling studies have also estimated the volume transport of different ISOW branches (labeled in magenta with parentheses in **Figure 1**). For example, Xu et al. (2010) estimate that the total transport of ISOW along the northwestern slope south of Iceland is 3.3 Sv. The cross-RR transport in the ISOW layer is estimated to be 1.2 Sv and the westward transport through the CGFZ is 1.9 Sv. Another modeling study (Chang et al., 2009) also gives the estimate of the ISOW layer transport west of the Maury Channel (1.5 Sv), within the Rockall Trough (2.2 Sv), and into

the WEB (4.6 Sv). Most of these model-based estimates compare fairly well with observational estimates except for the transport estimate into the WEB.

However, to our knowledge, there is to date no observational or modeling study that describes these ISOW branches from a Lagrangian perspective, nor one that investigates the time-varying relationship among the different ISOW branches. The current research aims at filling those gaps and intends to shed light on the similarities and differences between the Eulerian-based and Lagrangian-based studies of ISOW spreading pathways and transports.

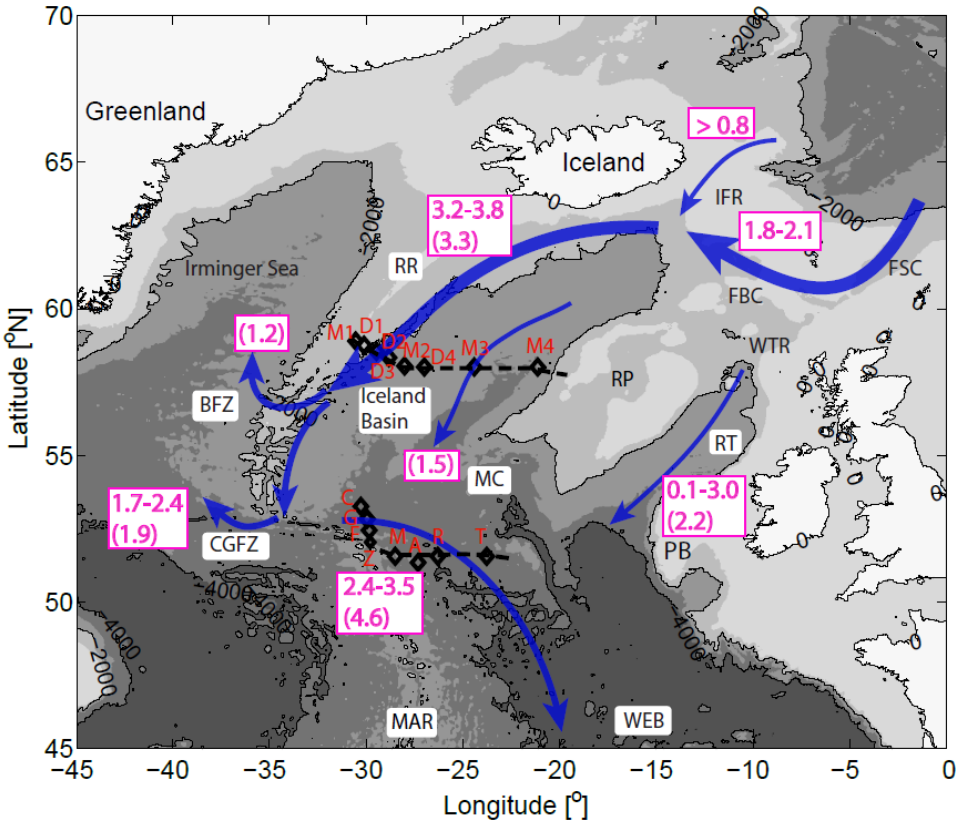

Figure 1. A schematic of the major ISOW spreading pathways, with black diamonds and dashed lines indicating the location of the moorings and CTD sections used in this study. Volume transports (unit: Sv) from previous Eulerian studies are labeled in magenta with those from models enclosed with parentheses. Abbreviations are: Iceland Faroe Ridge (IFR); Faroe-Shetland Channel (FSC); Faroe Bank Channel (FBC); Reykjanes Ridge (RR); Wyville-Thomson Ridge (WTR); Rockall Trough (RT); Rockall Plateau (RP); Porcupine Bank (PB); Bight Fracture Zone (BFZ); Charlie Gibbs Fracture Zone (CGFZ); Maury Chanel (MC); Mid-Atlantic Ridge (MAR) and West European Basin (WEB). All transport estimates shown here are from studies referenced in section 2.

3. Data and Methods

3.1 Mooring array and CTD stations in the central Iceland Basin

To identify ISOW and its transport cores in the Iceland Basin, we use a mooring array (M1, D1, D2, D3, M2, D4, M3 and M4 in **Figure 1)** and a set of CTD stations (black dashed line in **Figure 1**) across the Iceland Basin at 58-59°N. The mooring array and the CTD stations constitute part of the Overturning in the Subpolar North Atlantic Program (OSNAP) - East section, which extends from the southern tip of Greenland to Scotland (Lozier et al., 2016).

The mooring array was deployed in July 2014 across the entire Iceland Basin at depths between 699m and 2830m. Here we use the mean velocity and property profiles at depths ≥ 1000m from the first year of measurements to study the ISOW transport. On the same cruise, CTD measurements were conducted across the OSNAP section. CTD data at depths ≥ 1000m along the eastern flank of the RR, where the ISOW major branch is located, is also used in this study.

3.2 Mooring array and CTD stations east of CGFZ

Another mooring array used in this study is located to the east of the CGFZ. The moorings, labeled C, G, F, Z, M, A, R and T are shown in **Figure 1**. Moorings C, G, F and Z were deployed on June 25, 1999 and largely recovered on July 1, 2000. Moorings M, A, R and T were deployed on August 9, 1998 and recovered on June 16, 1999. All instruments were deployed at depths between 1650m and 3890m. The data used here is the annual mean velocity field at all instrumental depths. Additionally, CTD profiles conducted on FS METEOR in June 1999, when moorings M, A, R and T were recovered, are also used in this study.

3.3 RAFOS floats

Along the 2014 OSNAP cruise track in the Iceland Basin, acoustically tracked deep Range and Fixing of Sound (RAFOS) floats were released to study the ISOW spreading pathways (Lozier et al., 2016). In this paper, we use 9 floats that were initiated between 1800dbar and 2400dbar along the eastern flank of the RR. The initial launch locations and the trajectories of these floats can be found in **Figure 2-4**. These floats followed isobaric surfaces and had an approximate lifetime of two years.

Gaps in float positions, noted in **Figure 3-4**, possibly result from: 1) the blockage of the sound signal by a topographic feature, such as a seamount or bight; 2) the degradation of signal strength due to rough surface conditions; and/or 3) too great of a distance between the sound source and the float. As shown below, these gaps do not seriously impair our view of the floats' spreading pathways.

3.4 FLAME model

The model used in this paper is the eddy-resolving (1/12°) member of the Family of Linked Atlantic Models Experiment (FLAME) (Biastoch et al., 2008; Böning et al., 2006). The model

uses primitive equations and is spun up from rest with European Center for Medium-Range Weather Forecasts (ECMWF) climatological forcing for 10 years. After spin-up, the model is forced with monthly anomalies of NCEP/NCAR reanalysis data (Kalnay et al., 1996) superimposed on climatological forcing to create a hindcast dataset from 1990 to 2004. Climatological temperature and salinity are maintained at the open boundaries during the simulation.

The z-coordinate model has 45 levels in the vertical, with spacing increasing from 10m near the surface to 250m in the deep ocean. The domain spans from 18°S to 70°N on a Mercator grid. Data used in this paper are the temperature, salinity and three-dimensional velocity fields from 1990 to 2004, all with a temporal resolution of 3 days.

Several past studies have demonstrated FLAME's ability to reproduce observed property and velocity fields in the North Atlantic (Lozier et al., 2013; Gary et al., 2011). Additionally, the spreading pathways of the deep water masses simulated in FLAME are similar to those derived from observed floats (Bower et al., 2009; Getzlaff et al., 2006) and the eddy kinetic energy (EKE) fields at 15m in FLAME and from observations (altimetry and surface drifter velocity fields) show similar structure (Burkholder and Lozier, 2011). As shown below, FLAME is also capable of recreating the volume transport and spreading pathways of ISOW observed by mooring arrays and RAFOS floats. Therefore, in addition to the confidence in the model's ability to reproduce the general characteristics of the North Atlantic circulation, we consider FLAME highly suitable for analyzing ISOW transport pathways.

3.5 Simulated float launch configuration and trajectory computation

To compute trajectories, floats are initiated at specific locations defined by latitude, longitude and depth. Since our focus is on ISOW pathways, all floats are initiated in the ISOW layer, which is distinguished from the LSW layer by higher density and salinity. For density, we choose the threshold of 27.80 kg/m^3 in the Iceland Basin for both observations and FLAME, the same threshold applied in previous modeling (Xu et al., 2010; Chang et al., 2009) and observational studies (Kanzow and Zenk, 2014). FLAME salinities and densities are larger than observed, so the modeled isopycnal of 27.80 kg/m^3 is shallower than the observed isopycnal (shown below), resulting in a thicker ISOW layer in FLAME. Thus, to better distinguish the modeled ISOW layer, we also apply salinity thresholds in the range of [34.95, 34.98], which compare to observed thresholds in the range of [34.91, 34.94]). Our choice of isohalines to define ISOW depends on geographic locations, as well as time period. These choices are subjective and based on inspection of the salinity and density fields. Only when the float's initial density and salinity are greater than the thresholds is the float released.

From an initial launch position, float trajectories are computed using the three-dimensional velocity in FLAME, as detailed in Gary et al. (2011). To extend the lifetime of floats launched in the last few years of the model duration, we recycle the model velocity fields with a single discontinuity between December 31, 2004 and January 1, 1990, so that velocity fields on January 1, 2005 and onward are the same as January 1, 1990 and onward.

4 Spreading pathways of ISOW in the eastern North Atlantic

4.1 Escape of ISOW through gaps along the RR

To trace ISOW spreading pathways, we use observed and simulated floats initiated in the ISOW layer along the OSNAP section (58-59°N). **Figure 2** shows the cross-sectional salinity based on CTD stations in July 2014 (**left panel**) and the salinity across 58°N in FLAME averaged between 1990 and 2004 (**right panel**). Both observations and model output show the ISOW layer attached to the ridge, with fresh LSW occupying the interior basin at intermediate depths. The initial launch locations of the 9 RAFOS floats are shown as colored circles in **Figure 2 (left)**. To illustrate the different ISOW pathways, we divide the RAFOS floats into two subsets: one subset of floats was initiated at pressures of ~1800dbar (red circles) and the other was initiated at pressures greater than 2000dbar (blue circles). In this section, we focus on the first subset of the shallower floats.

Trajectories of the three shallower RAFOS floats are shown as black curves in **Figure 3**. Two of them escape into the Irminger Sea through the gaps in RR: one through the BFZ and one through the gap further south. The remaining float continues southward until the latitude of CGFZ.

Considering that RAFOS floats are limited in number, we turn to simulated floats to further illustrate this escape branch. Simulated floats were released in the shallower ISOW layer (< 1800m) along the RR eastern flank at 58°N every 3 months from 1990 to 2002 (red dots in **Figure 2, right**), and integrated forward by two years. The probability map of the two-year float trajectories is shown in **Figure 3**. The simulated pathways of the shallower ISOW are well aligned with those from RAFOS floats: a sizable number of floats escape to the Irminger Sea through BFZ and other gaps in the RR; the remaining floats primarily continue southward to the latitude of CGFZ.

In summary, based on observed and simulated float trajectories, the relatively shallow ISOW along the eastern RR flank can escape into the Irminger Sea through RR gaps before reaching the CGFZ, as previously noted in Eulerian modeling studies (Xu et al., 2010; Chang et al., 2009). This pathway is also shared by LSW, as illustrated with RAFOS floats studied by Lankhorst and Zenk (2006). A quantification of this pathway is addressed in section 5.

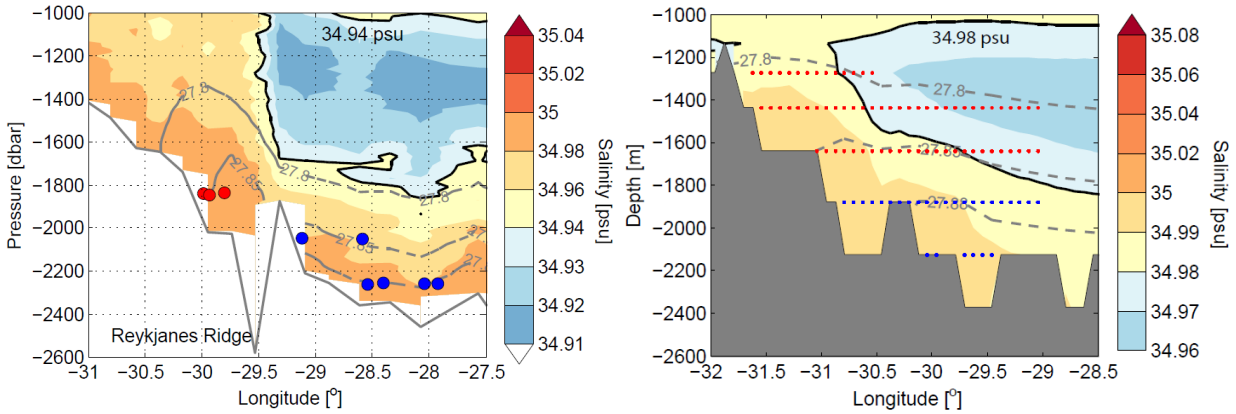

Figure 2. (Left) Observed salinity in July 2014 across the OSNAP section (58-59°N, black dashed line in **Figure 1**) along the eastern flank of the RR. The initial launch locations of the 9 RAFOS floats are plotted as colored circles (red and blue). Isohaline is shown in solid black and isopycnals are contoured as dashed gray lines. (Right) Modeled salinity averaged from 1990 to 2004 across 58°N. Dots in the right panel show the initial launch locations of simulated floats. All floats were initiated in the ISOW layer defined by the property field at launch, which is different from the 15-year mean shown in this panel. Therefore, though some dots appear in the fresh LSW layer, they were in ISOW when they were initiated. Note that the salinity color scale is different between the two panels.

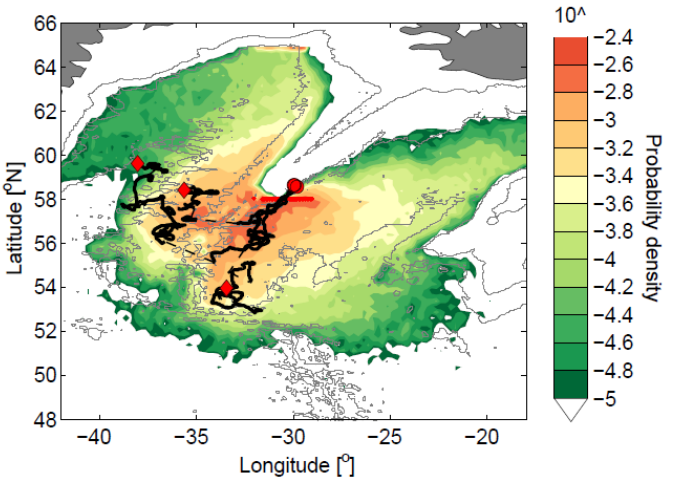

Figure 3. Pathways of shallow ISOW from the eastern flank of the RR at 58°N. Two-year trajectories of three RAFOS floats are plotted in thick black curves with their initial (final) locations shown as red circles (diamonds). The thin dashed lines connect the gaps where float positions are missing. Probability map of simulated trajectories of shallow ISOW is shaded in color underneath the RAFOS trajectories. Floats were released every three months from 1990 to 2002 and were integrated forward by two years. The probability is computed by dividing the North Atlantic into 0.25°×0.25° grids, counting the number of times floats pass through each grid (including repetitions), and then dividing the number of passes in each grid by the total float passes over all grids (Gary et al., 2012; Zou and Lozier, 2016). The probabilities shown here are on a log scale. 4234 simulated floats were launched along the red short line (also shown in **Figure 2, right**). 1000m, 2000m and 3000m isobaths are contoured in light gray.

4.2 Westward spreading of ISOW through the CGFZ

The second subset of RAFOS floats (6 in total) released at greater depths (blue circles in **Figure 2, left**) reveals a different spreading pathway. Instead of crossing the RR gaps into the Irminger Sea, all 6 floats move southward along the eastern RR flank. Essentially, these floats are too deep to cross the RR gaps, such as the BFZ (~2030m). Along this southward route, two of the floats turn eastward into the basin interior (**Figure 4**). The remaining 4 floats continue moving southward,

with three reaching the CGFZ. Interestingly, after reaching the CGFZ, two floats immediately turn southward along the western flank of the MAR and one float travels westward. None of the floats show northward spreading along the western RR boundary. This interesting feature is under investigation in a related, but separate study (A. Bower, personal communication).

Again, we turn to modeled floats for a more complete illustration. The launch strategy is similar to that in section 4.1, except that the floats were released at greater depths (> 1800m) (blue dots in **Figure 2, right**). **Figure 4** shows the probability map of the simulated deep ISOW spreading pathways within two years. While a small amount escapes through the RR gaps, the majority of the simulated deep ISOW follows similar pathways observed by RAFOS floats. It first flows southward and then either turns into the basin interior or continues southward to the latitude of CGFZ, where westward crossing and southward spreading along the western MAR are both seen. A primary difference is that the modeled trajectories reveal a weak southward spreading of ISOW into the WEB, which is not observed by RAFOS floats. One possible reason for this difference is that the RAFOS floats are too few in number to have sampled this branch. Another reason is that, as will be shown in the next section, the primary origin of waters within this southward branch is the interior and eastern portion of the Iceland Basin, yet the RAFOS floats were released along the western part of the basin.

Westward transport across the CGFZ has been shown to be impacted by meridional shifts of the NAC (Schott et al., 1999; Bower and Furey, 2017). For example, Bower and Furey (2017) show that on eddy time scales, a strong westward ISOW transport across the CGFZ is observed when there is a southward shift of the NAC: when the NAC approaches the northern channel of the CGFZ, the transport in the ISOW layer is eastward. To test whether NAC's shift has a similar impact on ISOW transport on interannual time scales, we plot the annual cross-sectional zonal velocity across the CGFZ in 1996 and 2003 (**Figure 5**). The former year is when the Eulerian-based westward ISOW transport in the model is the strongest during the decade and the latter year is when the transport is the weakest.

In 1996, the NAC almost disappears in the upper water column of the CGFZ northern channel. Instead, a bottom intensified westward velocity is seen. In 2003, a branch of eastward NAC overlies a weak westward ISOW transport, but this shift is less evident compared to what is observed by Bower and Furey (2017) on eddy time scales. Though the model behavior appears to be consistent with what has been inferred from Bower and Furey (2017), further work is needed to assess the dependence of ISOW transport variability on NAC variability on interannual time scales.

In summary, deep ISOW along the RR eastern flank mainly flows southward until the CGFZ, where some continues spreading southward along either side of the MAR and some crosses westward into the western subpolar gyre. The westward crossing varies on both eddy time scales and interannual time scales, apparently in concert with NAC interactions. Within two years from 58°N, very few floats flow northward along the western RR boundary after reaching CGFZ.

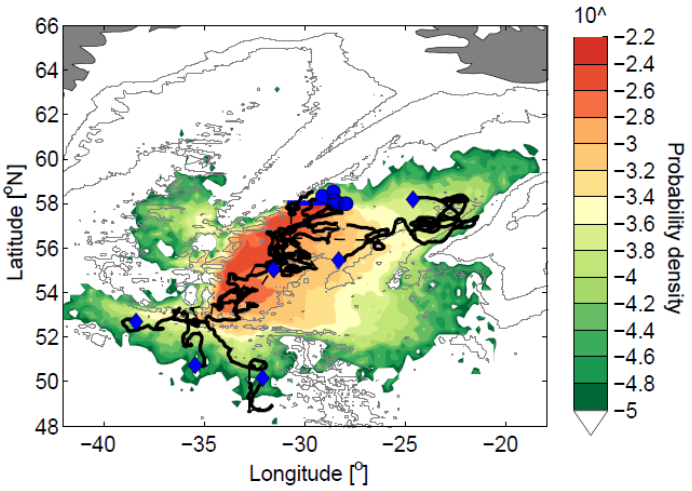

Figure 4. Similar to **Figure 3**, but for pathways of ISOW originated at greater depths. The initial (final) positions of the 6 RAFOS floats are shown as blue circles (diamonds). The initial launch locations of simulated floats are shown with a blue short line at 58°N. The total float number is 2534.

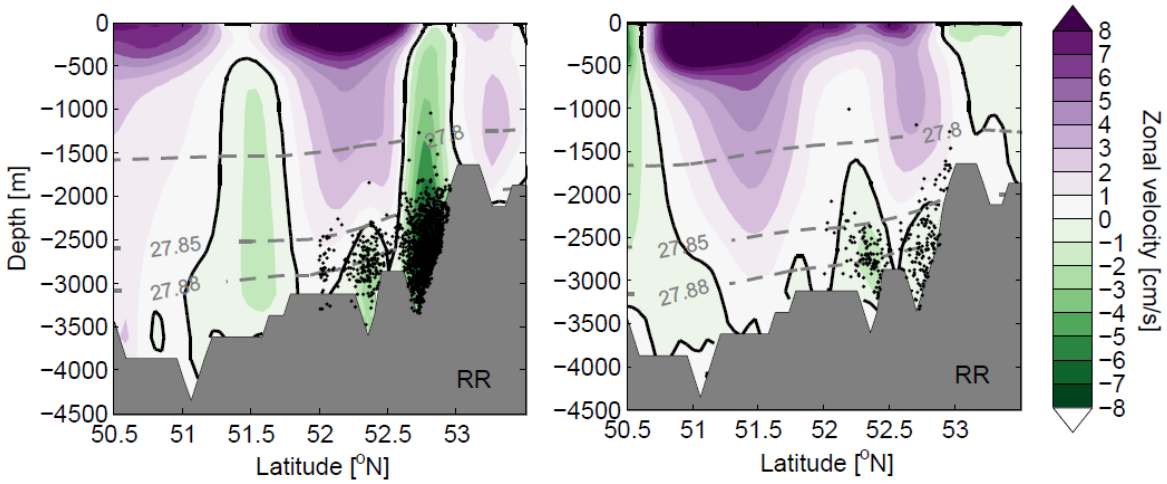

Figure 5. (Left) Annual mean zonal velocity across the CGFZ in 1996. The float positions while crossing the fracture zone in 1996 are plotted as black dots. (Right) Similar to the left panel, but for the mean zonal velocity across CGFZ in 2003. The zero velocity contour is shown in black. Isopycnals are contoured in dashed gray.

4.3 The southward spreading of ISOW into the WEB along the eastern flank of the MAR

The third ISOW export pathway discussed in this paper is a southward spreading into the WEB east of the MAR. Here we present previously unpublished current meter observations that measure this deep southward transport. **Figure 6 (left)** shows the mean velocity at mooring locations C, G, F and Z (deployed from June 1999 to July 2000) and M, A, R and T (deployed from August 1998 to June 1999) at instrument depths between 1650 and 3890m. The deep-reaching northeastward

NAC is observed at moorings G, F and Z. At mooring R, a bottom-intensified southward flow is observed in both the salty ISOW layer and the relatively fresh LDW layer near the bottom, as shown by the hydrographic section from CTD casts conducted in June 1999 (**Figure 6, right**). The southward velocity increases from 1.7 cm/s to 6.1 cm/s in the ISOW layer and reaches 8 cm/s in the LDW layer.

The modeled annual mean velocity in 1998, when moorings M, A, R and T were in water, is indicated with blue arrows in **Figure 7 (left),** with the cross-sectional meridional velocity at 51.5°N shown in **Figure 8 (left)**. Also shown is the annual mean velocity field in 1992, when the southward velocity is the strongest of all model years (**Figure 7 left, green arrows; Figure 8, right**). Overall, though the southward velocities in the ISOW layer (**Figure 7, right**) are evident near moorings A and R in FLAME for both years, their magnitudes are much weaker than observations. The bottom intensification of the observed velocity at mooring R is also not evident in FLAME, suggesting an underestimate of the southward spreading in the model.

The meridional velocity fields at 51.5°N shown in **Figure 8** also reveal significant variability from year to year in the model, which might result from the meandering or the position shift of the NAC. To test whether the velocity fields impact the southward ISOW spreading, we released simulated floats in the ISOW layer in 1998 and in 1992. The two-year probability maps of float trajectories for each of these launches are shown in **Figure 9**. In 1998, when the southward velocity is relatively weak, the floats prefer to travel northeastward towards the Rockall Plateau (**Figure 9, left**). However, in 1992, when the southward velocity is relatively strong at 51.5°N, a southward spreading pathway emerges (**Figure 9, right**). This southward pathway is consistent with the southward movement of a RAFOS float launched in the ISOW layer (2600 dbar) east of the CGFZ, as reported by Lankhorst and Zenk (2006). The track of this RAFOS float is also shown in **Figure 9**.

We note that although a southward spreading of deep waters is observed along the MAR eastern flank, it is difficult to ascertain the waters' source. LSW from the western subpolar gyre, subtropical water carried by the NAC, LDW from the south and ISOW from the Iceland Basin are all expected components of the deep water in this region. To study the possible origins of these deep waters, we computed backward trajectories of simulated floats released every 3 months in 1992 at 51.5°N near the moorings M, A and R. The probability maps (**Figure 10)** from this launch reveal that the primary source of the deep waters in this area is the interior Iceland Basin, with another important origin east of the Flemish Cap, where eastward-flowing LSW meets waters carried by the NAC. Based on these model results and current knowledge about the North Atlantic subpolar gyre circulation, we conclude that the waters moving southward along the eastern MAR flank are a composite of subpolar water masses, with ISOW a strong contributor. This conclusion is consistent with an Eulerian study by Xu et al. (2010).

In summary, from both observations and FLAME output, a southward spreading of ISOW into the WEB is identified east of the MAR. However, in FLAME, this southward spreading appears much weaker and is temporally variable depending upon the local velocity field, which has been suggested to be influenced by NAC meandering (Bower and Furey, 2017).

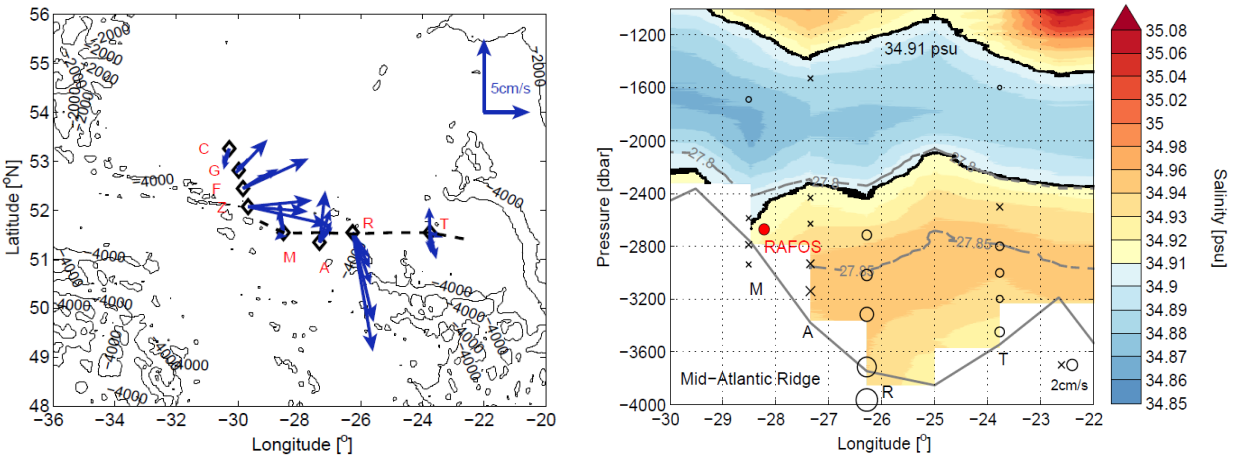

Figure 6. (Left) Mean velocities at the depths of all current meters for moorings C, G, F, Z, M, A, R and T (black diamonds). Moorings C, G, F and Z were deployed on June 25 1999 and recovered on July 1 2000. Moorings M, A, R and T were deployed on August 9 1998 and recovered on June 16 1999. All current meters are located between 1650 and 3890 dbar. The CTD section is shown as a black dashed line. (Right) Observed salinity in June 1999 east of the MAR (~51.5°N) from the CTD stations shown in the left panel. The depths of the current meters for each mooring are marked as black circles if the mean velocity is southward and crosses if the mean velocity is northward, with size proportional to the current speed. A few markers are below the bottom (gray solid line) due to the longitude difference between the mooring locations and the CTD section. The red circle indicates the approximate location of the RAFOS float when it crossed 51.5°N. Isopycnals are shown as dashed gray contours.

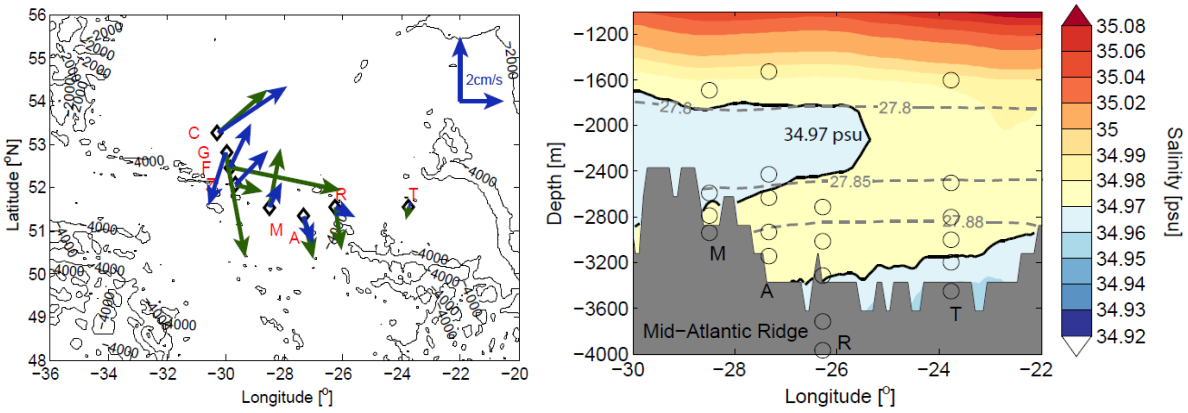

Figure 7. (Left) Annual mean velocity from FLAME in 1998 (dark blue) and 1992 (dark green), at mooring locations. The velocity is averaged over the ISOW layer. Mooring locations are indicated with black diamonds. (Right) Modeled salinity averaged from 1990 to 2004 across 51.5 °N. The longitudes of the moorings M, A, R and T are shown as black circles. Isohalines are shown in solid black and isopycnals are contoured as dashed gray lines.

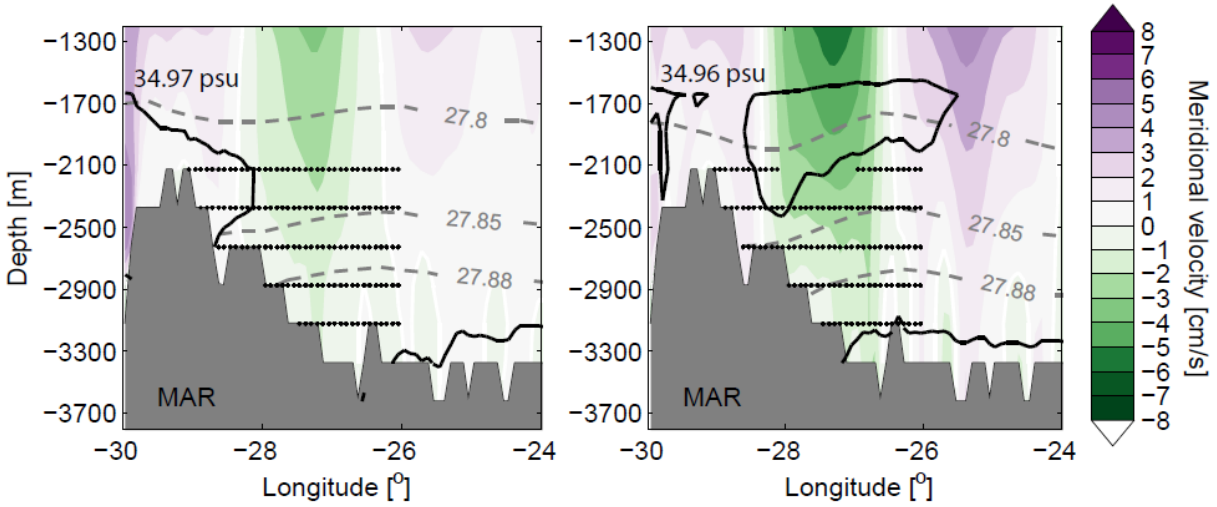

Figure 8. The annual mean meridional velocity across 51.5°N in FLAME in 1998 (left) and 1992 (right). Black solid contour shows the isohaline and the gray dashed contours indicate isopycnals. Black dots indicate the launch locations of simulated floats along 51.5°N.

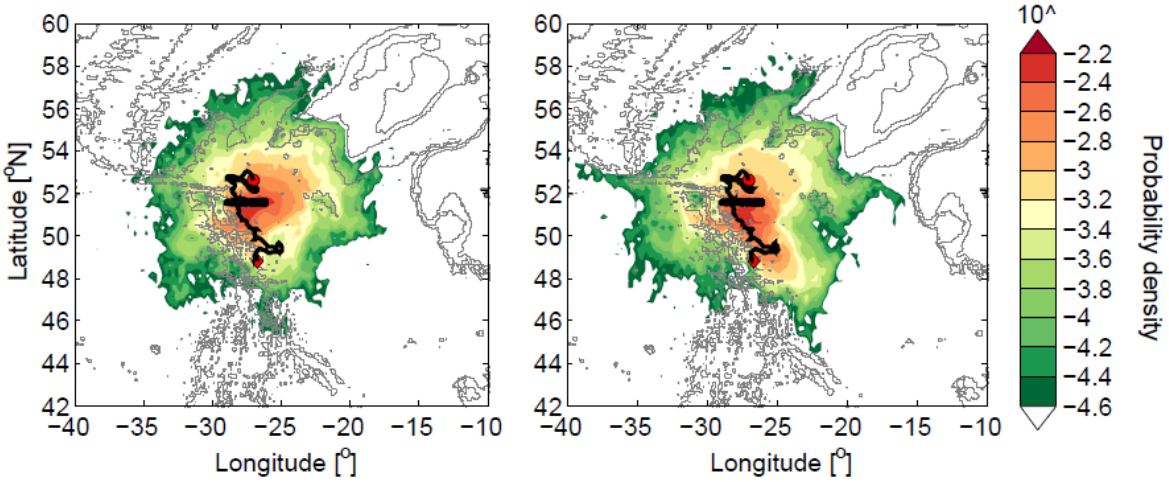

Figure 9. Probability maps of float trajectories two years after release in 1998 (left) and 1992 (right) at 51.5°N in FLAME. 2824 floats were released every 3 months in the ISOW layer in 1998 and 2650 were released in 1992. Initial launch locations are shown in black (also in **Figure 8**). A RAFOS float trajectory is shown as a black solid curve with its initial (final) location denoted by a red circle (diamond). The RAFOS float data is obtained from Lankhorst et al. (2017).

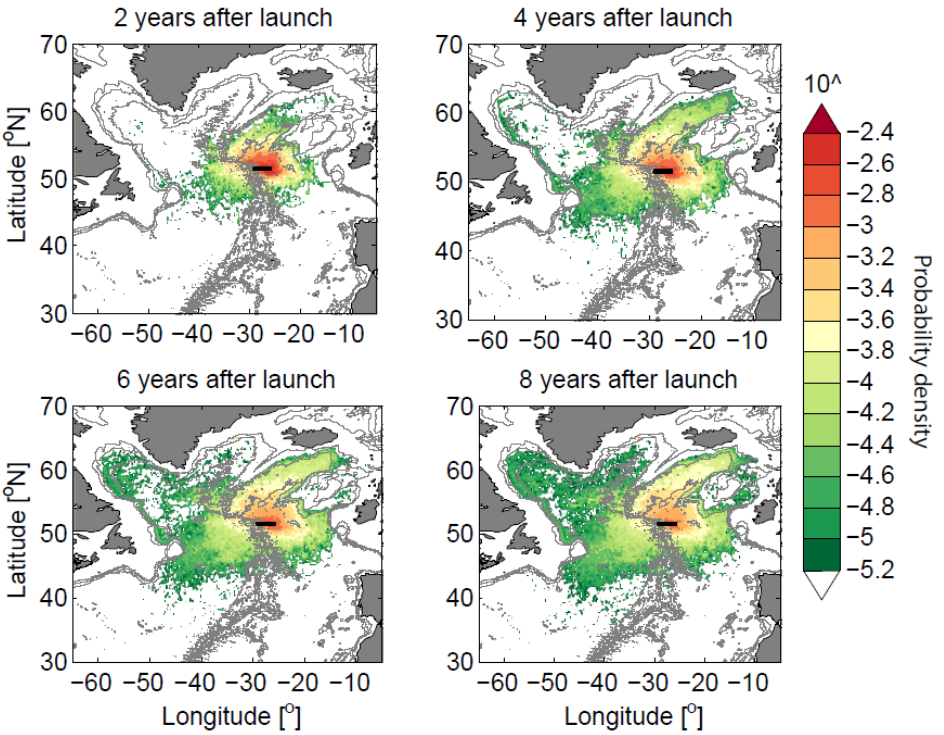

Figure 10. Probability maps of backward trajectories of floats released every 3 months in 1992 in the ISOW layer at 51.5°N (black short line).

4.4 An overall view of ISOW spreading pathways from the Iceland Basin

In order to identify ISOW across the entire Iceland Basin, we use current meter and hydrographic data from the OSNAP mooring array and data from FLAME. The observed mean velocities (July 2014-July 2015) at depths ≥ 1000m are shown in red in **Figure 11,** along with the 15-year mean volume transport in the layer below the isopycnal of 27.80 kg/m^3 in FLAME. The vertical structure of the velocity field at the observational array and from FLAME are shown in **Figure 12**. Overall, the modeled velocity structure compares fairly well with observations: they both reveal bottom-intensified southward velocity cores near the mooring locations (one core near moorings M1, D1 and D2, one near D4 and another near M3). A difference between the model and observations is noted: in the model, the bottom southward flow field is much weaker at moorings D3 and M2, and reverses directions at mooring M4. The difference at mooring M4 can perhaps be attributed to the fact that the observations were conducted during 2014 and 2015 while FLAME spans only from 1990 to 2004. For example, the flow direction near mooring M4 does change from year to year in FLAME (e.g. the velocity at M4 is northward in 2003, not shown). The weak velocities at moorings D3 and M2 in the model are present every year, revealing the shortcoming of FLAME in capturing the entire boundary current east of the RR. However, ISOW in the high velocity core of the boundary current is well resolved in the model, and this branch is the major ISOW transport branch.

To study the overall ISOW spreading, we released floats every 3 months in 1990 in the bottom-intensified southward velocity cores in the ISOW layer identified above. The two western cores

near M1-D2 and near D3 are clearly associated with southward ISOW flow from the northern Iceland Basin, while the core near M3 appears to be at least partly associated with a localized deep circulation cell in the model in the eastern part of the basin. These floats were released across 59°N, a latitude close to the mooring section and one that captures the southward ISOW transport cores (**Figure 13, left**). After launch, floats were integrated forward for 10 years.

From the probability map of 10-year trajectories of exported floats (**Figure 13, right)**, we easily recognize the strong recirculation of ISOW in the Iceland Basin and the three major export pathways discussed above: one branch crosses into the Irminger Sea via gaps along RR, while another branch spreads southward along the eastern RR flank until the CGFZ area, where it bifurcates into a westward pathway through the CGFZ and a pathway continuing southward along the eastern flank of the MAR. There is also a relatively weak southward spreading of the floats along the western flank of the MAR. Launches in years other than 1990 were performed; no discernable difference in the overall spreading pathways was detected.

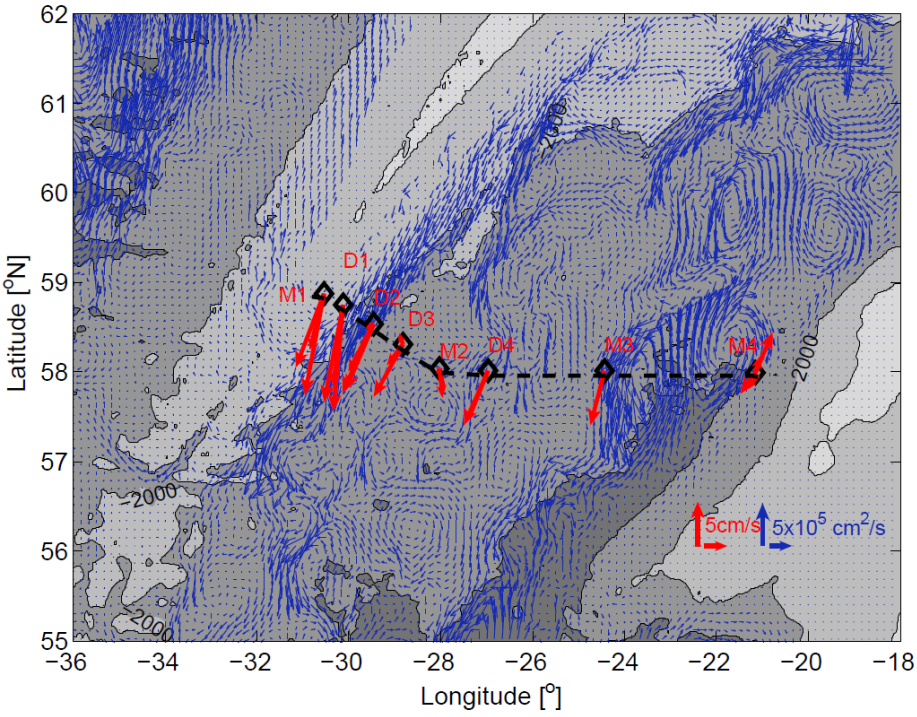

Figure 11. Annual mean velocity (red arrows) from current meter data at all observed depths. Locations of mooring M1, D1, D2, D3, M2, D4, M3, and M4 are shown with black diamonds. All moorings were deployed in July 2014 and recovered in July 2015. Blue arrows show the 15-year mean volume transport per unit width (product of velocity and layer thickness, unit: cm^2/s) for the layer below the isopycnal of 27.80 kg/m^3. Black dashed line shows the section in FLAME that replicates the mooring site. 1000m, 2000m and 3000m isobaths are shown in gray.

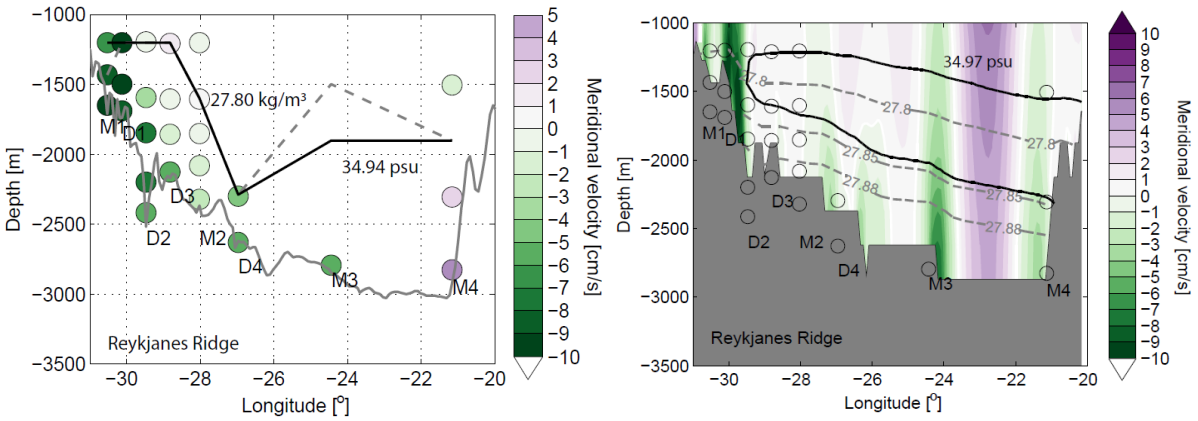

Figure 12. Comparison of the mean velocity structure between observations and FLAME across the OSNAP section. (Left) Mean meridional velocity from OSNAP moorings between July 2014 and July 2015, with bathymetry shown by the gray line. The 27.80 kg/m^3 isopycnal and 34.94 isohaline are plotted in solid black and gray dashed lines, respectively. Note that the salinity and density for each mooring array are measured with CTDs, which occupy more vertical layers than current meters. (Right) Mean meridional velocity averaged from 1990 to 2004 in FLAME along the section that replicates the OSNAP array (black dashed line in **Figure 11**). The vertical distributions of the OSNAP current meters are shown in open circles. Isopycnals are contoured in dashed gray and the isohaline is contoured in sold black. Modeled bathymetry is shaded in dark gray. A few deep open circles are located in the gray area due to the coarse resolution of bathymetry in FLAME.

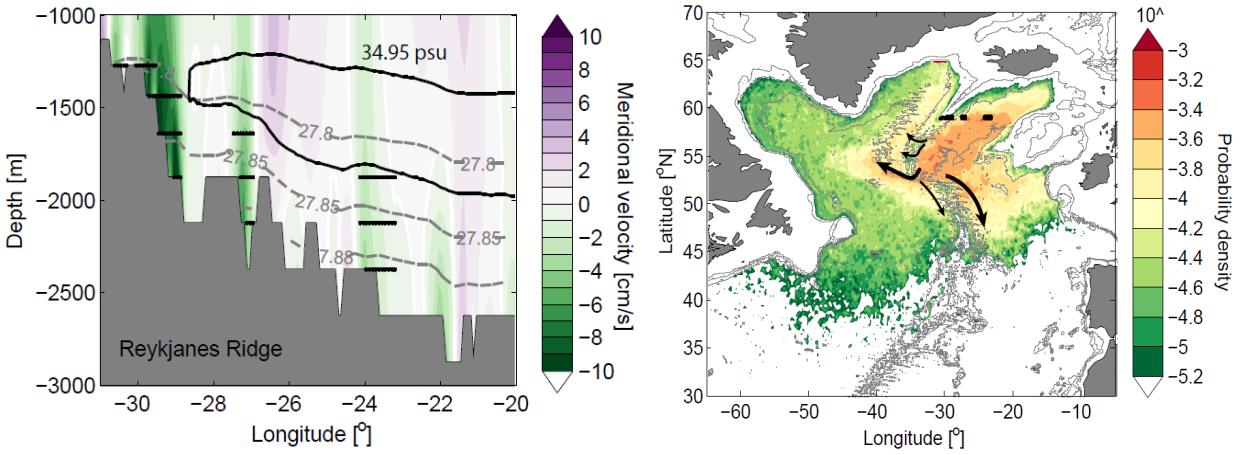

Figure 13. (Left) Annual mean meridional velocity across 59°N in 1990 from FLAME. Initial launch locations of floats are shown as black dots. (Right) Probability map of 10-year trajectories of exported floats (1227 in total). Floats were released every 3 months in 1990 in the southward velocity cores at 59°N. Only floats whose final locations are outside of the Iceland Basin are used for this plot. Floats' initial locations are shown as black dots at 59°N. Major ISOW export branches are illustrated with black solid curves. 1000m, 2000m and 3000m isobaths are shown in gray.

5 Quantitative distribution of ISOW through different pathways

In this section, we use FLAME to calculate the annual volume transport of ISOW in the eastern North Atlantic, and compare those transports to results from previous observational and modeling studies. In FLAME, the mean (1990-2004) of the annual alongshore transport of ISOW along the slope south of Iceland (~62°N) is 3.8 Sv, with a standard deviation of 0.7 Sv (labeled in blue in **Figure 14**). As it flows southward, this branch splits into two branches that remain near the boundary. A third southward branch of ISOW is located west of the Maury Channel in the basin interior. This branch, with a transport of 1.8 ± 0.7 Sv, has no obvious connection to the ISOW branch south of Iceland and instead appears part of a local circulation feature. The net southward transport in the interior Iceland Basin east of 26°W, which includes this third branch, is 0.4 ± 0.4 Sv. Summing all transports, we derive a net southward transport in the ISOW layer across the entire Iceland Basin at 59°N of 4.2 ± 0.5 Sv.

The cross-RR transport between 60°N and CGFZ is calculated as 1.2 ± 0.1 Sv and the transport across the CGFZ is 0.9 ± 0.4 Sv. Finally, the net throughput of deep waters into the WEB is 2.8 ± 0.7 Sv. Most of these modeled transports compare favorably with previous studies (values in magenta in **Figure 14**). We point out the mismatch in transport through the CGFZ and suggest that part (though certainly not all) of this mismatch may be attributed to the subjective choice of the salinity threshold for ISOW the layer in the model. Appropriate choices for this threshold yield a range of mean transports from 0.8 Sv to 1.3 Sv, with the latter closer to previous transport estimates.

To understand the source of the waters constituting each of these branches, we turn again to a Lagrangian perspective. We released floats every 3 months each year from 1990 to 2004 in FLAME across 59°N in the Iceland Basin (red dashed line in **Figure 14**) and integrated forward by 10 years. Floats were released each year in the ISOW layer regardless of whether the initial velocity was northward or southward. We are interested in the export of floats across the red solid lines marked in **Figure 14**, selected to designate the destinations of the three identified spreading branches. Thus, we use these sections to measure export. For example, if a float crosses the red solid section along the RR axis sometime within 10 years of launch, and by the end of the 10^{th} year it remains in the western North Atlantic, this float is considered to have been exported through the RR. With this accounting, we obtain the number of exported floats through each section (RR, CGFZ and east of MAR) from each launch year. We convert those numbers to percentages by dividing by the total number of initial floats launched (4860 ± 950, float number varies in different years as ISOW layer thickness varies).

The percentage of each branch increases almost linearly with time of integration (not shown). As seen in **Figure 14**, 10 years after launch, the fraction exported across the RR is 7%, with a standard deviation of 1% among all launches. The fraction exported across the CGFZ is 13 ± 2% and east of the MAR is 21 ± 3%. The southward export of ISOW along the eastern flank of the MAR is more significant compared to the other two export pathways. The distribution is slightly different if we release floats only within the mean southward velocity cores across 59°N: 11 ± 1% across the RR; 10 ± 2% through the CGFZ; and 18 ± 2% along the eastern flank of the MAR. Also, a small portion (4 ± 0.5 %) of the floats flow southward along the western flank of the MAR. Most

of the remaining floats are un-exported, meaning that they remain in the Iceland Basin during this 10-year period.

Float export variability through the different sections as a function of their initial launch years is shown in **Figure 15**. The percentage of southward export along the eastern flank of the MAR is negatively correlated with the export percentage via RR gaps (r = -0.75 before detrending; r = -0.66 after detrending). The correlation primarily stems from opposite trends (**Figure 15, left**) and anti-phase variability on semi-decadal time scales (**Figure 15, right**). A negative correlation is also seen between the southward export east of the MAR and the westward export across the CGFZ, with a correlation coefficient of -0.38 before detrending and -0.83 after detrending. The strong negative correlation between the two detrended time series results from the anti-phase variability on interannual time scales. If we add the export percentage via the RR gaps and through the CGFZ, the total is significantly anti-correlated with the southward export pathway east of the MAR (r = -0.78 before detrending; r = -0.91 after detrending), indicating that when cumulative ISOW transport across RR gaps and the CGFZ is relatively strong, southward ISOW transport into the WEB is weak. One should note that since we are recycling the data to get the 10-year float trajectories for launches after 1995, the export variability derived here might not reflect the real export variability from year to year. However, this work sheds light on the potential relationship between different pathways in exporting ISOW out of the Iceland Basin.

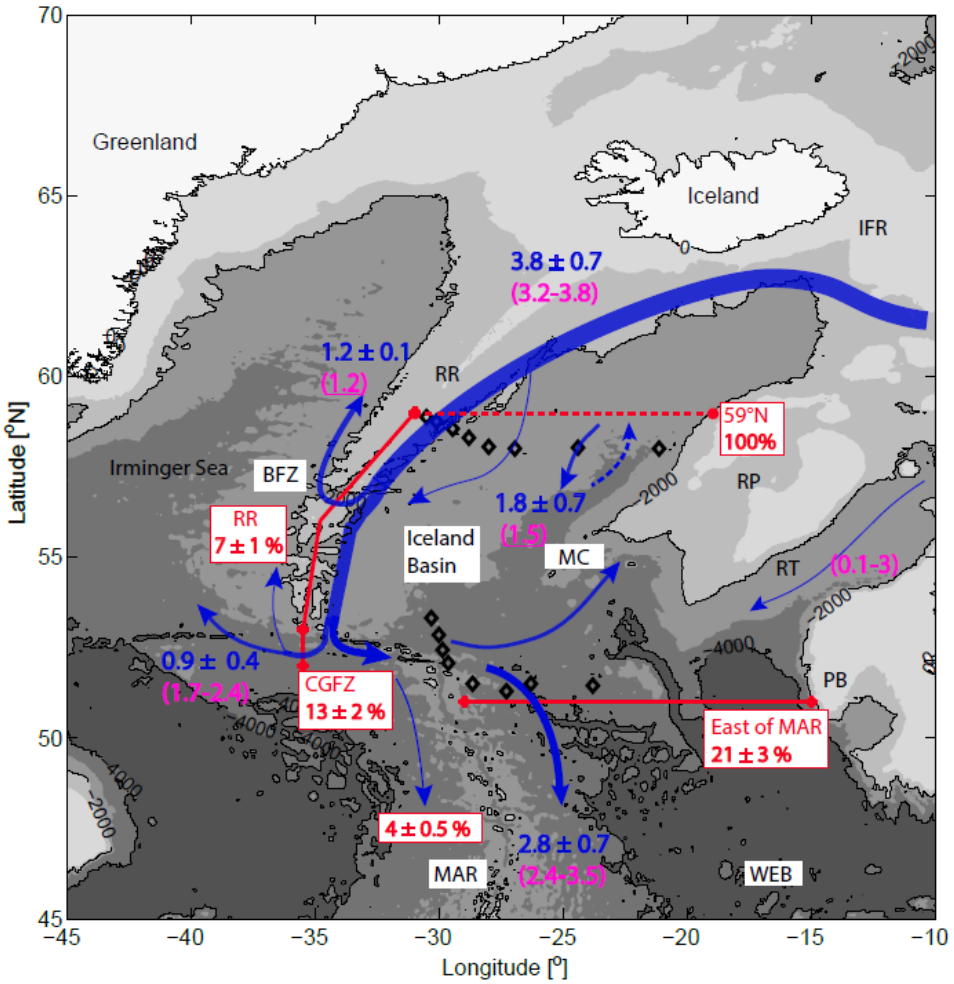

Figure 14. Mean pathways (blue curves) for ISOW in the eastern North Atlantic in FLAME. Volume transports (Sv) for major branches from the model are labeled in blue. The transport values from previous studies are listed in magenta within parentheses, with those from modeling studies underlined. The percentage of exported floats within 10 years after release at 59°N (red dashed line) through different sections (RR, CGFZ, east of MAR) is shown in red. Mooring arrays used in this paper are plotted as black diamonds.

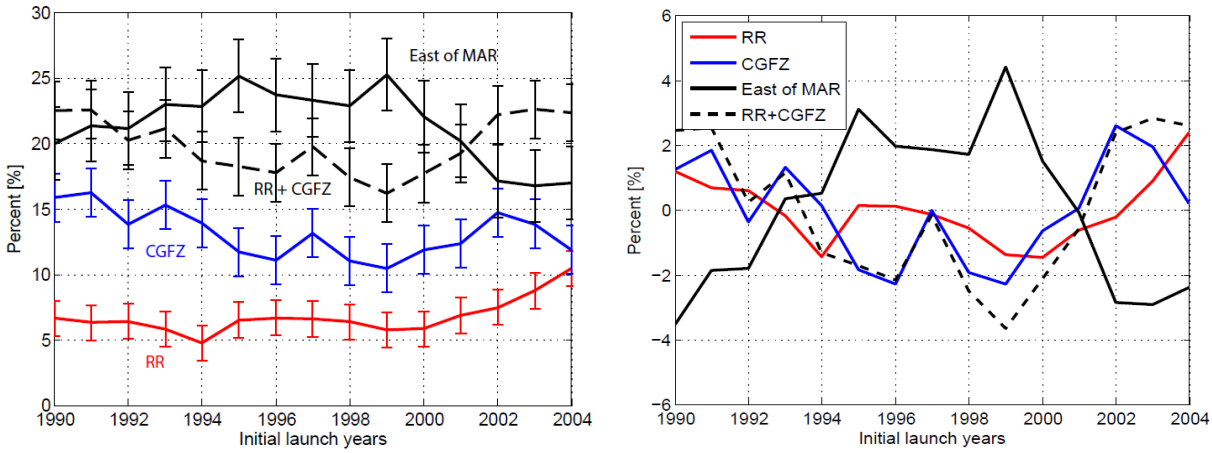

Figure 15. Export variability expressed as a percentage of floats through different sections within 10 years after release in the ISOW layer across the entire basin at 59°N. (Left) Before detrending. The standard deviation is shown as an error bar. (Right) After detrending. Export percentages from studies where floats were released only in the southward velocity cores at 59°N show similar variability to the time series shown above.

6 Conclusions

Earlier studies of the ISOW pathways in the eastern North Atlantic have relied on model output and/or limited observations; in both cases pathways were inferred using an Eulerian framework. In this study, for the first time, we use a combination of Eulerian and Lagrangian approaches, and a combination of observations and high-resolution numerical model output, to trace and quantify ISOW spreading branches.

After entering the Iceland Basin, ISOW primarily travels along the eastern flank of the RR, with some ISOW flowing to the basin interior. When it reaches 59°N, three ISOW transport cores are identified from an OSNAP mooring array and from model output: one major core is along the RR boundary; another weaker core is in the basin interior at ~27°W; and the third one resides in the eastern basin at ~24°W, appearing to be part of a local circulation cell. With observed and simulated trajectories, the spreading branches of ISOW from these transport cores are identified. A portion of shallow ISOW along the RR eastern boundary escapes to the Irminger Sea via gaps along the Ridge (modeled volume flux: 1.2 ± 0.1 Sv) before reaching the CGFZ. The remaining ISOW, either along the boundary or from the basin interior, primarily flows southward to the CGFZ, where one branch of this deep water crosses westward into the western subpolar gyre (modeled volume flux: 0.9 ± 0.4 Sv) and another continues spreading southward into the WEB (modeled volume flux: 2.8 ± 0.7 Sv). While these export branches are consistent with previous Eulerian studies, they are identified here with Lagrangian floats for the first time. Furthermore, this study provides the first direct observational validation of the southward branch into the WEB, a validation possible due to the examination of previously unpublished current meter data. In addition to the identification of the major export pathways mentioned above, Lagrangian floats

reveal a weak southward spreading along the western flank of the MAR and strong recirculation of the remaining ISOW in the Iceland Basin.

A quantification of different ISOW branches in a modeled Lagrangian frame reveals that downstream of 59°N in the Iceland Basin after 10 years, 7-11% of ISOW escapes the basin via RR gaps; 10-13% flows into the western subpolar gyre through the CGFZ; and 18-21% continues moving southward into the WEB along the eastern flank of the MAR. In other words, the export via RR gaps and through the CGFZ are comparable, while the southward export east of the MAR is more significant. Most of the remaining ISOW (~50%) stays in the Iceland Basin 10 years following launch. A small portion (4%) exports along the western flank of the MAR. Note that these float percentages indicate preferred ISOW pathways from 59°N over the course of 10 years, a different metric than the volume transport at a fixed location.

From our modeling experiments, we find that the southward ISOW transport percentage into the WEB and the westward ISOW transport percentage through the CGFZ have strong interannual variability. In both cases, this variability appears linked to the variability of the NAC in the magnitude and/or position. Further work is needed to confirm the dynamic link between them.

Changes in the modeled pathways are shown to be interrelated. An increase of the total ISOW export percentage across the RR gaps and through the CGFZ is associated with a decrease in the southward transport percentage to the WEB on interannual time scales as well as on longer time scales. On interannual time scales, this association is driven by the relationship between the CGFZ transport and the southward transport: when the westward CGFZ transport is relatively strong, the southward transport into the WEB is relatively weak, and vice-versa. On longer time scales, the transport through the RR gaps is more important to this linkage.

With this work, we have provided an overall view of the ISOW spreading pathways and confirmed them to the extent possible with observations. However, we still lack an understanding of the variability of these transport pathways and the mechanisms responsible for that variability. As more OSNAP data becomes available in the next few years, we expect gaps in that understanding to diminish.

Acknowledgements

The authors gratefully acknowledge the Physical Oceanography Program of the U.S. National Science Foundation and Deutsche Forschungsgemeinschaft in Bonn, Germany for the support of this work. Gratitude is also extended to colleagues who graciously shared data and/or codes: Matthias Lankhorst and Olaf Boebel for RAFOS float data; Claus Böning and Arne Biastoch for FLAME data; Heather Furey for OSNAP RAFOS float data; and Stefan Gary for float trajectory computation code.

References

Beaird, N. L., P. B. Rhines, and C. C. Eriksen. 2013. Overflow Waters at the Iceland–Faroe Ridge Observed in Multiyear Seaglider Surveys. Journal of Physical Oceanography 43:2334-2351.

Biastoch, A., C. W. Böning, J. Getzlaff, J.-M. Molines, and G. Madec. 2008. Causes of Interannual–Decadal Variability in the Meridional Overturning Circulation of the Midlatitude North Atlantic Ocean. Journal of Climate 21:6599-6615.

Böning, C. W., M. Scheinert, J. Dengg, A. Biastoch, and A. Funk. 2006. Decadal variability of subpolar gyre transport and its reverberation in the North Atlantic overturning. Geophysical Research Letters 33.

Bower, A. S., B. L. Cann, T. Rossby, W. Zenk, J. Gould, K. Speer, P. L. Richardson, M. D. Prater, and H-M. Zhang. 2002. Directly measured mid-depth circulation in the northeastern North Atlantic Ocean. Nature 419, no. 6907: 603-607.

Bower, A. S., M. S. Lozier, S. F. Gary, and C. W. Boning. 2009. Interior pathways of the North Atlantic meridional overturning circulation. Nature 459:243-247.

Bower, A. S., and H. Furey. 2017. Iceland-Scotland Overflow Water transport variability through the Charlie-Gibbs Fracture Zone and the impact of the North Atlantic Current. Journal of Geophysical Research: Oceans.

Burkholder, K. C., and M. S. Lozier. 2011. Subtropical to subpolar pathways in the North Atlantic: Deductions from Lagrangian trajectories. Journal of Geophysical Research 116.

Chang, Y. S., Z. D. Garraffo, H. Peters, and T. M. Özgökmen. 2009. Pathways of Nordic Overflows from climate model scale and eddy resolving simulations. Ocean Modelling 29:66-84.

Curry, R. G., M. S. McCartney, and T. M. Joyce. 1998. Oceanic transport of subpolar climate signals to mid-depth subtropical waters. Nature 391:575-577.

Daniault, N., H. Mercier, P. Lherminier, A. Sarafanov, A. Falina, P. Zunino, F. F. Pérez, A. F. Ríos, B. Ferron, T. Huck, V. Thierry, and S. Gladyshev. 2016. The northern North Atlantic Ocean mean circulation in the early 21st century. Progress in Oceanography 146:142-158.

Dickson, R. R., and J. Brown. 1994. The production of North Atlantic Deep Water: Sources, rates, and pathways. Journal of Geophysical Research 99:12319.

Eldevik, T., J. E. Ø. Nilsen, D. Iovino, K. Anders Olsson, A. B. Sandø, and H. Drange. 2009. Observed sources and variability of Nordic seas overflow. Nature Geoscience 2:406-410.

Ellett, D. J., and D. G. Roberts. 1973. The overflow of Norwegian sea deep water across the Wyville-thomson Ridge. Deep Sea Research and Oceanographic Abstracts 20:819-835.

Fleischmann, U., H. Hildebrandt, A. Putzka, and R. Bayer. 2001. Transport of newly ventilated deep water from the Iceland Basin to the Westeuropean Basin. Deep Sea Research Part I: Oceanographic Research Papers 48:1793-1819.

Gary, S. F., M. S. Lozier, A. Biastoch, and C. W. Böning. 2012. Reconciling tracer and float observations of the export pathways of Labrador Sea Water. Geophysical Research Letters 39(24).

Gary, S. F., M. S. Lozier, C. W. Böning, and A. Biastoch. 2011. Deciphering the pathways for the deep limb of the Meridional Overturning Circulation. Deep Sea Research Part II: Topical Studies in Oceanography 58:1781-1797.

Getzlaff, K., C. W. Böning, and J. Dengg. 2006. Lagrangian perspectives of deep water export from the subpolar North Atlantic. Geophysical research letters 33.21.

Hansen, B., and S. Østerhus. 2007. Faroe Bank Channel overflow 1995–2005. Progress in Oceanography 75:817-856.

Hansen B., KMH. Larsen, H. Hátún, and S. Østerhus, 2016. A stable Faroe Bank Channel overflow 1995-2015. Ocean Science 12: 1205–1220, doi:10.5194/os–12–1205–2016.

Kalnay, E., M. Kanamitsu, R. Kistler, W. Collins, D. Deaven, L. Gandin, M. Iredell, S. Saha, G. White, J. Woollen, Y. Zhu, A. Leetmaa, R. Reynolds, M. Chelliah, W. Ebisuzaki, W. Higgins, J. Janowiak, K. C. Mo, C. Ropelewski, J. Wang, R. Jenne, and D. Joseph. 1996. The NCEP/NCAR 40-Year Reanalysis Project. Bulletin of the American Meteorological Society 77:437-471.

Kanzow, T., and W. Zenk. 2014. Structure and transport of the Iceland Scotland Overflow plume along the Reykjanes Ridge in the Iceland Basin. Deep Sea Research Part I: Oceanographic Research Papers 86:82-93.

Lankhorst, M., and W. Zenk. 2006. Lagrangian Observations of the Middepth and Deep Velocity Fields of the Northeastern Atlantic Ocean. Journal of Physical Oceanography 36:43-63.

Lankhorst, M., Nielsen, M., Zenk, W., 2017: RAFOS Float Data in the Northeast Atlantic 1997-2003 from the SFB460 Project. PANGAEA Dataset.
https://doi.pangaea.de/10.1594/PANGAEA.874240

Lavender, K. L., W. Brechner Owens, and R. E. Davis. 2005. The mid-depth circulation of the subpolar North Atlantic Ocean as measured by subsurface floats. Deep Sea Research Part I: Oceanographic Research Papers 52:767-785.

Lozier, M. S., S. Bacon, A. S. Bower, S. A. Cunningham, M. F. de Jong, L. de Steur, B. deYoung, J. Fischer, S. F. Gary, B. J. W. Greenan, P. Heimbach, N. P. Holliday, L. Houpert, M. E. Inall, W. E. Johns, H. L. Johnson, J. Karstensen, F. Li, X. Lin, N. Mackay, D. P. Marshall, H. Mercier, P. G. Myers, R. S. Pickart, H. R. Pillar, F. Straneo, V. Thierry, R. A. Weller, R. G. Williams, C. Wilson, J. Yang, J. Zhao, and J. D. Zika. 2016. Overturning in the Subpolar North Atlantic Program: a new international ocean observing system. Bulletin of the American Meteorological Society.

Lozier, M. S., S. F. Gary, and A. S. Bower. 2013. Simulated pathways of the overflow waters in the North Atlantic: Subpolar to subtropical export. Deep Sea Research Part II: Topical Studies in Oceanography 85:147-153.

Machín, F., U. Send, and W. Zenk. 2006. Intercomparing drifts from RAFOS and profiling floats in the deep western boundary current along the Mid-Atlantic Ridge. Scientia Marina 70.1: 1-8.

McCartney, M. S. 1992. Recirculating components to the deep boundary current of the northern North Atlantic. Progress in Oceanography 29:283-383.

Molinari, R. L., R. A. Fine, W. D. Wilson, R. G. Curry, J. Abell, and M. S. McCartney. 1998. The arrival of recently formed Labrador sea water in the Deep Western Boundary Current at 26.5°N. Geophysical Research Letters 25:2249-2252.

Rudels, B., H. J. Friedrich, and D. Quadfasel. 1999. The Arctic Circumpolar Boundary Current. Deep Sea Research Part II: Topical Studies in Oceanography 46:1023-1062.

Saunders, P. M. 1994. The flux of overflow water through the Charlie-Gibbs Fracture Zone. Journal of Geophysical Research 99:12343.

Saunders, P. M. 1996. The Flux of Dense Cold Overflow Water Southeast of Iceland. Journal of Physical Oceanography 26:85-95.

Schott, F., L. Stramma, and J. Fischer. 1999. Interaction of the North Atlantic Current with the Deep Charlie Gibbs Fracture Zone Throughflow. Geophysical Research Letters 26:369-372.

Schott, F. A., J. Fischer, M. Dengler, and R. Zantopp. 2006. Variability of the Deep Western Boundary Current east of the Grand Banks. Geophysical Research Letters 33.

Sherwin, T. J., and W. R. Turrell. 2005. Mixing and advection of a cold water cascade over the Wyville Thomson Ridge. Deep Sea Research Part I: Oceanographic Research Papers 52:1392-1413.

Sherwin, T. J., C. R. Griffiths, M. E. Inall, and W. R. Turrell. 2008. Quantifying the overflow across the Wyville Thomson Ridge into the Rockall Trough. Deep Sea Research Part I: Oceanographic Research Papers 55.4: 396-404.

Stramma, L., D. Kieke, M. Rhein, F. Schott, I. Yashayaev, and K. P. Koltermann. 2004. Deep water changes at the western boundary of the subpolar North Atlantic during 1996 to 2001. Deep Sea Research Part I: Oceanographic Research Papers 51.8: 1033-1056.

van Aken, H. M. 1995. Hydrographic variability in the bottom layer of the Iceland Basin. Journal of physical oceanography, *25*(7), 1716-1722.

van Aken, H. M., and C. J. De Boer. 1995. On the synoptic hydrography of intermediate and deep water masses in the Iceland Basin. Deep Sea Research Part I: Oceanographic Research Papers 42:165-189.

Xu, X., P. B. Rhines, E. P. Chassignet, and W. J. Schmitz. 2015. Spreading of Denmark Strait Overflow Water in the Western Subpolar North Atlantic: Insights from Eddy-Resolving Simulations with a Passive Tracer. Journal of Physical Oceanography 45:2913-2932.

716 Xu, X., W. J. Schmitz, H. E. Hurlburt, P. J. Hogan, and E. P. Chassignet. 2010. Transport of
717 Nordic Seas overflow water into and within the Irminger Sea: An eddy-resolving simulation and
718 observations. Journal of Geophysical Research 115.

719 Zou, S., and M. S. Lozier. 2016. Breaking the Linkage Between Labrador Sea Water Production
720 and Its Advective Export to the Subtropical Gyre. Journal of Physical Oceanography 46:2169-
721 2182.

722